NonlinearÀLinear Transition of Magnetoelectric Effect in Magnetic Graphene Nanoflakes on Substrates

ARTICLE *in* THE JOURNAL OF PHYSICAL CHEMISTRY C · NOVEMBER 2012

Impact Factor: 4.77 · DOI: 10.1021/jp205841z

THE JOURNAL OF PHYSICAL CHEMISTRY C

ARTICLE

pubs.acs.org/JPCC

Nonlinear−Linear Transition of Magnetoelectric Effect in Magnetic Graphene Nanoflakes on Substrates

Peng Lu,[†] Zhuhua Zhang,*[,†] C. H. Woo,[‡] and Wanlin Guo*[,†]

[†]Institute of Nano Science and Key Laboratory of Intelligent Nano Materials and Devices of Ministry of Education, Nanjing University of Aeronautics and Astronautics, Nanjing 210016, China

[‡]Department of Electronic and Information Engineering, The Hong Kong Polytechnic University, Hong Kong SAR, China

ABSTRACT: Linear magnetoelectric (ME) effect provides an ideal way to control magnetism by an external electric field and has long been pursued in spintronics. However, the essential conditions for linear ME effects are still not well understood, especially for the newly emerged metal-free ME systems. Here, using density functional theory calculations, we reveal a novel nonlinear−linear transition of the ME effect in graphene nanoflakes (GNFs) placed on substrates with different chemical activities. We show that the ME effect is nonlinear in a magnetic GNF on graphene substrate. Interestingly, the ME effect in the same GNF becomes highly linear with markedly increased ME coefficient when an *h*-BN sheet is inserted between the GNF and graphene layer. We reveal that the weak electronic hybridization between the GNFs and substrate is the essential mechanism for the linear ME behavior in the graphene-based magnets. The tunable nonlinear−linear transition in ME coupling opens up new opportunities to fabricate and manipulate high-quality ME devices.

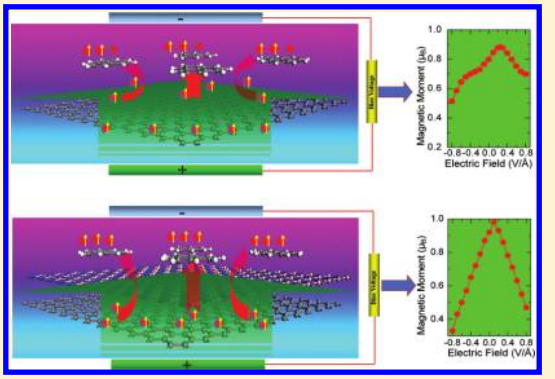

1. INTRODUCTION

The magnetoelectric (ME) effect, the induction of magnetization by means of an electric field and induction of polarization by means of a magnetic field,[1,2] has become one of the most intensively studied issues due to its great promise in technical applications.[3−8] The applications of ME effect include transducers, magnetic field sensors, and the industrially demanding information storage technology. In the past decades, the ME effect studies mainly focus on the materials containing d or f electrons, such as the $SrRuO_3$,[1] $TbMnO_3$,[4] $HoMnO_3$,[5] Fe,[6] and other related metal oxide heterostructures.[7,8] To achieve higher storage density with lower expense, using metal-free magnets, especially the newly emerged carbon-based magnets, may be an alternative solution. However, the progress in extending the ME effect into these metal-free magnets is relatively retarded. To this end, it is quite encouraged to see that the ME effect has been predicted in zigzag graphene nanoribbons (ZGNRs) settled on silicon substrates,[9,10] offering new insight into the applications of ME devices. Nevertheless, ZGNRs have one-dimensional flat edges and are just a tip of the iceberg of various magnetic graphene structures. Actually, a more general form of graphene structures is the graphene nanoflake (GNF),[11−22] which is finite in both the dimensions and whose edge shapes can be tailored more flexibly according to the applications. Many theoretical predictions have shown that the GNFs could possess large spins depending on its shape and the topological frustration of the conjugated electronic states,[11−22] in contrast to GNRs that actually have zero net spins because of the antiferromagnetic coupling between two opposite ferromagnetic edges. Such magnetic GNFs of single atom thickness will even become technologically important, because the individual elements of future electronics or spintronics devices will certainly continue to shrink to sustain the trend of enhanced performance. Therefore, exploring the ME effect in magnetic GNFs is not only essential to measure the transferability of the new ME mechanism proposed in ref 9 but may also provide an important step toward realizing practical ME devices. On the other hand, the linear ME effect is known to be well suited for control of magnetic devices. Nevertheless, it is still unclear as to what is the essential condition for the linear ME effect in graphene-based magnets. So it is also necessary to explore the physical mechanism underlying the linear ME behavior and clarify whether there are some ways to regulate the ME effect between nonlinear and linear behaviors.

Here, we demonstrate through first-principles calculations a nonlinear−linear transition of ME effect in GNFs on lamellar substrates. We show that a bias-induced nonlinear ME effect is obtained when the GNF is directly placed on graphene layers due to the strong interlayer interaction. Interestingly, the ME effect is tuned to be linear and the ME coefficient is greatly enhanced when a chemically inert hexagonal BN sheet is sandwiched between the graphene and magnetic GNF. We identify that the interaction between the substrate and GNF plays a dominant role in determining the ME behaviors. Our findings underscore the

Received: June 22, 2011
Revised: November 9, 2011
Published: November 14, 2011

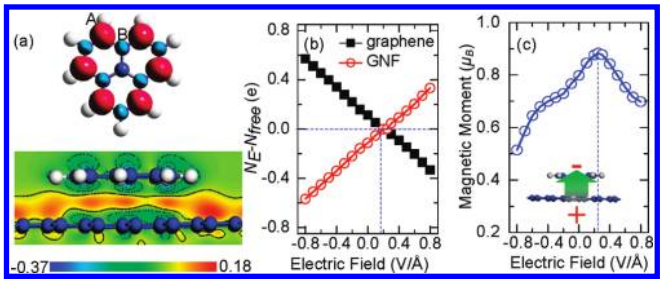

Figure 1. (a) Top: Magnetization density of graphene nanoflake (GNF, $C_{13}H_9$), magenta (dark) and light blue (gray) colors represent spin-up and -down directions, respectively. Bottom: charge redistributions induced by adsorption of the GNF and graphene. Red and blue colors indicate charge accumulation and depletion regions, respectively. The contour spacing is uniformly set to be 80×10^{-3} e/Å^3. (b) Amounts of transferred electrons in the graphene and GNF as a function of electric field strength. (c) Net magnetic moment of the GNF as a function of the electric field strength. Insert is the atomic structure of the GNF on graphene substrate with bias electric field. Green and gray balls represent carbon and hydrogen atoms, respectively.

importance of choosing suitable intermediate layers in designing high-quality ME devices.

2. COMPUTATIONAL METHOD

First-principles calculations are performed using the Vienna ab initio simulation package (VASP) code.[23−25] Ultrasoft pseudopotentials for the core region and local spin density approximation (LDA) for the exchange-correlation potential are used. This is because LDA can give reasonable interlayer spacing between graphene layers that is an important factor in our study, while general gradient approximate (GGA) fails to do this. A kinetic energy cut of 530 eV is used in the planewave expansion. The calculated model consists of one magnetic GNF lying on a graphene or a hexagonal BN layer, with all the dangling bonds terminated by hydrogen atoms. The atoms under each applied bias voltage are relaxed by conjugate gradient method until the force on each atom is less than 0.02 eV/Å, which is enough for convergent local magnetization in the GNF. With regard for the calculations of magnetic moment in GNFs, we find that both GGA and LDA calculations give nearly the same results. The Wigner Seitz radiuses of carbon and hydrogen atoms are set to be 1.208 and 0.423 Å, respectively, and they can affect the GNF moment dramatically. However, the magnitude of net moment will only affect some quantitative aspects of our discussion but are not expected to change any conclusions on trends and mechanisms. We consider a vacuum region of 12 Å to avoid the interaction between two adjacent images. Two-dimensional Brillouin-zone integration is sampled by up to 16 special *k*-points for structural optimization. The external electric field is introduced by planar dipole layer method as implemented in VASP. In addition, the ground state of GNF is calculated using the Becke and Lee−Yang−Parr (B3LYP) exchange correlation functional[26] and the 3-21G basis set, as implemented in the Gaussian03 package.[27]

3. RESULTS AND DISCUSSION

3.1. Structural and Electronic Properties of GNFs. Magnetic GNFs have been extensively investigated theoretically and experimentally.[11−22] For the consideration of computational limits, we first take the possible smallest magnetic GNF, formulated as $C_{13}H_9$, for a model system to show the ME effect and essential physics. We will show later that our results are a universal character in all magnetic GNFs. The atomic configuration of the freestanding GNF, is shown in Figure 1a. The GNF consists of three benzene rings arranged in a triangular form. The magnetic moment of the GNF is 1.00 μ_B, and the magnetic state is more stable by 0.11 eV than the nonmagnetic state. This is corroborated by our additional calculations using Gaussian package, which show that the ground state of the GNF is in the doublet state. The spin-polarized electrons with spin-up and -down directions are distributed on the atoms belonging to A and B sublattices, respectively, as shown in Figure 1a. The calculated total spin magnetic moment of the GNF is in good agreement with the predictions of Lieb's theorem[28] and former work[29] with Hubbard model for bipartite lattices.

3.2. Nonlinear ME Effect in GNF with Graphene Substrate. First, we use a single-layered graphene[30] as the substrate, on which the GNF is placed. The GNF interacts with the graphene layer through weak interlayer $\pi-\pi$ orbitals interaction, which results in an optimized interlayer distance of 3.22 Å, slightly smaller than 3.3 Å in a freestanding bilayer graphene system.[31] Note that there is also long-ranged van der Waals interaction, which, however, does not refer to electronic states. Upon formation of the stacked system, we find that the electrostatic potential in the GNF plane is lower than that in the graphene plane. Such difference in electrostatic potential drives a spontaneous charge transfer about 0.13 *e* from the GNF to graphene (Figure 1a). As a result, the total magnetic moment of the GNF is reduced to 0.85 μ_B, while the graphene shows *n*-doped character. In the following discussion, we will focus on the total change in the GNF moment and do not consider their components because of the small nonlinear effect for spins in GNFs as a result of the very weak spin−orbit coupling effect and the hyperfine interaction in carbon.

We thus apply an external electric field to control the charge transfer, which, in turn, should result in electrically controlled magnetic moment in the GNF. We define the electric field along the normal of the graphene as a positive direction (insert of Figure 1c). Because of inherent charge transfer between the graphene and GNF, the graphene changes from *n*-doped to *p*-doped at bias voltage around 0.25 V/Å. As shown in Figure 1b, the amount of electrons transferred from graphene to the GNF increases linearly from 0 to 0.33 *e* with the bias voltage changing from 0.25 to 0.8 V/Å, rendering the graphene substrate *p*-doped. On the other side, with the bias voltage changing from 0.25 to −0.80 V/Å, the amount of electrons transferred from GNF to the graphene increases linearly from 0 to 0.57 *e* and the graphene substrate becomes *n*-doped. Concomitant with the variable charge transfer, the net magnetic moment of the GNF increases from 0.51 to 0.88 μ_B with the bias voltage changing from −0.80 to 0.25 V/Å and decreases from 0.88 to 0.70 μ_B with the bias voltage increasing from 0.25 to 0.80 V/Å, both in a nonlinear manner. This forms a sharp contrast with the results in ref 9, where the linear ME effects are revealed in both the *n*- and *p*-doped region. By scrutinizing Figure 1c, one can find that the linear ME coupling occurs only in certain ranges of applied bias voltage, namely, −0.80 to −0.60 V/Å, −0.60 to −0.10 V/Å, −0.20 to 0.25 V/Å, 0.25 to 0.70 V/Å, and 0.70 to 0.80 V/Å (Figure 1c). In the whole range of bias voltage from −0.80 to 0.80 V/Å, the ME coupling shows a remarkable character of nonlinearity.

To explore the origin of different ME coupling behaviors in different regions of bias voltage, we plot the spin-polarized band

dx.doi.org/10.1021/jp205841z |J. Phys. Chem. C 2012, 116, 626–631

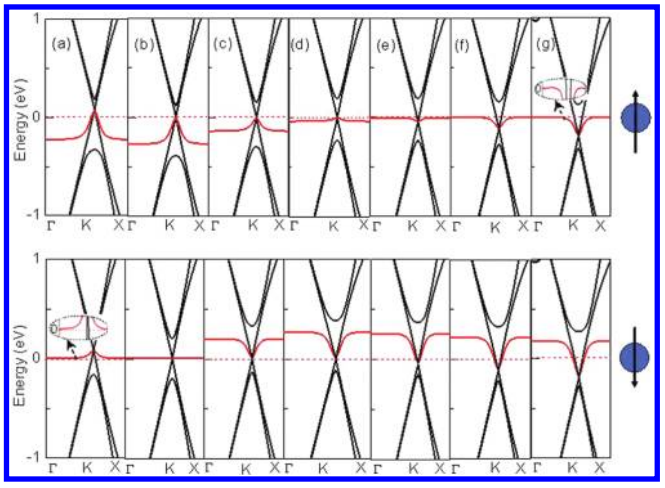

Figure 2. Spin-resolved band structures of the GNF ($C_{13}H_9$) on graphene substrate under bias voltages (a) 0.80 V/Å, (b) 0.60 V/Å, (c) 0.25 V/Å, (d) 0 V/Å, (e) −0.20 V/Å, (f) −0.40 V/Å, and (g) −0.60 V/Å. The cases of spin-up and spin-down are shown in the top and bottom panels, respectively. In the vicinity of the Fermi level, the bands contributed by the GNF are highlighted in red lines.

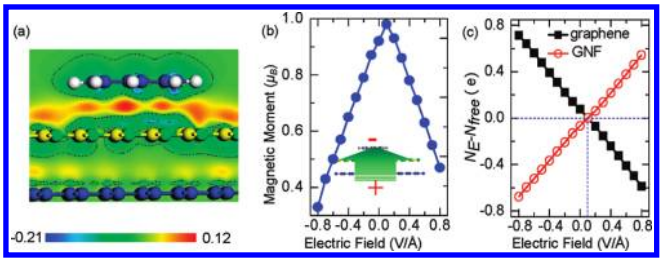

Figure 3. (a) Charge redistributions induced by adsorption of the GNF ($C_{13}H_9$), BN sheet, and graphene. Red and blue colors indicate charge accumulation and depletion regions, respectively. The contour spacing is uniformly set to be 80×10^{-3} e/Å^3. (b) Net magnetic moment of GNF as a function of electric field strength. Insert is the atomic structure of the GNF on BN−graphene substrates with bias electric field. (c) Amounts of transferred electrons in the graphene and GNF as a function of electric field strength. Blue, green, yellow, and gray balls represent carbon, nitride, boron, and hydrogen atoms, respectively.

structures of the system under different bias voltages in Figure 2. The flat bands contributed by the GNF are highlighted in red lines. Induced by interlayer π interaction, the flat bands of GNF intercross with graphene bands and shift with the Dirac point under bias voltages. When the bias voltage changes from −0.20 to 0.70 V/Å, the Dirac point just cuts the Fermi level in the spin-polarized band structure,[32] and the spin-up and spin-down bands splitting from the flat states locate above and below the Fermi level, respectively (parts b−d of Figures 2). In the range of bias voltage from −0.20 to 0.25 V/Å, the electrons transferred to graphene are almost from the spin-down state of the GNF. As the GNF magnetization is proportional to the number difference between spin-up and spin-down electrons, the linear variation in transferred charge induces positive linear ME coupling in this bias range. Similarly, in the range of bias voltage from 0.25 to 0.70 V/Å, the electrons transferred from the graphene to GNF dominantly fill the spin-up state of GNF, thus producing a negative linear ME coupling.

The situation is changed when the bias voltage is between −0.20 and −0.6 V/Å or above 0.7 V/Å. We first take the bias region of −0.20 to −0.60 V/Å as an example. In this bias region, the Dirac point no longer cuts the Fermi level. Instead, a part of the spin-up flat band of GNF becomes lower than the Fermi level, implying that the spin-up electrons are transferred from the GNF to graphene (parts e and f of Figure 2). As such, transferred electrons from the spin-up states also make a contribution to the change in the net magnetic moment, due to the presence of mixed states around the Fermi level, although the varied population in the spin-down states still dominates the moment change. As a result, a nonlinear ME modulation is produced in this bias range. The emerged mixed states from spin-up channel are just due to the interlayer interaction of GNF with the graphene substrate, as will be proved later. The nonlinear behavior has similar origin once the bias voltage is larger than 0.70 V/Å, except for that a few mixed spin-down states instead emerge around the Fermi level (Figure 2a). When the negative bias voltage goes below −0.60 V/Å, the flat spin-down band of GNF becomes higher than the Fermi level, so that the varied population in the spin-up states is very tiny to contribute the variation of magnetic moment. Consequently, linear ME effect of GNF is restored in the bias range of −0.60 to −0.80 V/Å. In brief, a relative shift of the flat bands of GNF with respect to the Dirac point, which stems from the interlayer interaction, determines the different behaviors of ME coupling in different regions of bias voltage.

3.3. Linear ME Effect in GNFs with BN−Graphene Substrate. To further verify the interlayer interaction in determining the ME behavior, we also calculate the binding energy for the GNF on graphene substrate. It is shown that the binding energy for the GNF is 0.04 eV/atom, which is remarkably larger than 0.02 eV/atom for the second ZGNR in ref 10. So, decreasing the binding energy between the GNF and graphene should weaken the planar π interaction and thus may pose a linear ME effect in GNF. This is indeed the case that a linear ME effect emerges when we increase the distance between the GNF and graphene to 6.00 Å, at which with the binding energy lowered to 0.004 eV/atom. These calculations suggest that the interlayer interaction between the GNF and graphene dominates the ME behavior in the GNF by bias voltages.

Then it becomes important to regulate the ME effect into linear behavior in a practical system, since the linear ME effect is much favored for practical applications. It is well-known that the single-layered *h*-BN sheet has similar structure with the graphene sheet, and has been successfully prepared in the laboratory.[33] Particularly, experiment has also reported the assembly of graphene on the *h*-BN sheet substrate and showed that the supported graphene has properties almost identical to the case of freestanding.[34] Motivated by this result, we attempt to inset a single-layered *h*-BN sheet between the magnetic GNF and the graphene layer. As such, the interlayer interaction to GNF is mainly from the BN substrate and hence is small when compared to the GNF−graphene system, because the BN sheet is electronically very inert. In this system, the interaction between the GNF and the graphene layer is greatly diminished due to the large distance between them as well as the insertion of BN layer.

The corresponding equilibrium geometry for such system is shown in Figure 3a. Here, the optimized average equilibrium interlayer distance is 3.10 Å between the GNF and BN sheet, and 3.40 Å between the BN sheet and graphene. In this case, there is only 0.075 *e* transferred from GNF to graphene at zero voltage, and the magnetic moment on of GNF is 0.90 μ_B, very close to its

freestanding value. Upon the applied bias voltages, the critical bias voltage for *n*-to-*p* transition of graphene is reduced to 0.10 V/Å. Importantly, the ME effect in the GNF indeed becomes decently linear as shown in Figure 3b with changing the bias voltage from 0.80 to −0.80 V/Å, in stark contrast to the ME behavior in the aforementioned GNF−graphene system. The net moment of the GNF increases from 0.33 to 0.98 μ_B with bias voltage from −0.80 to 0.10 V/Å but decreases from 0.98 to 0.46 μ_B with bias voltage from 0.10 to 0.80 V/Å.

The dependence of induced magnetization ΔM on the applied electric voltage E is $\mu_0 \Delta M = \alpha E$,[6,9] where α denotes the ME coefficient. From the linear fit to the calculated data in Figure 3b, the ME coefficients are 3.67×10^{-12} G cm^2/V and -3.78×10^{-12} G cm^2/V in the *p*- and *n*-doped regions of GNF, respectively. These values are significantly larger than the equivalent values in the case of GNF−graphene system, where the approximate ME coefficients are only 1.42×10^{-12} G cm^2/V and -1.71×10^{-12} G cm^2/V in the *p*- and *n*-doped regions of GNF, respectively (Figure 1c). For comparison, the ME coefficients found here are tens of times higher than that obtained in recently discovered ferromagnetic metal films.[6] Note that the revealed ME effect based on the total change in magnetization vs applied electric field has been accepted by the community.[6,35] In fact, the ME effect has received a broader understanding. Many related phenomena such as an electrically controlled exchange bias[36] and magnetocrystalline anisotropy[37,38] and the effect of ferroelectricity on spin transport[39,40] can all be categorized into generalized ME effect.

To understand the enhanced ME effect, we first study the amounts of transferred electrons between the GNF and graphene as a function of the electric field strength, in Figure 3c. It is shown that the bias-induced charge transfer here is markedly enhanced when compared to the GNF−graphene system. The amounts of depleted and accumulated charges in the GNF achieve up to 0.74 and 0.61 *e* at bias voltages of −0.8 V/Å and 0.8 V/Å, respectively. The enhanced charge transfer is ascribed to the increased GNF−graphene distance that reduces the screening effect of electric field, and it directly magnifies the ME effect in the GNF layer. However, we find that the *h*-BN sheet exchanges very few amounts of electrons with the GNF and graphene. For example, at bias voltage of −0.8 V/Å, the amounts of accumulated charges are 0.54 *e* in the graphene but only 0.05 *e* in the BN sheet, thereby rendering the BN sheet to act as a dielectric layer.

To further identify whether the linear ME behavior is from the attenuated interlayer interaction felt by the magnetic GNF, we examine the charge redistribution between the GNF and BN plus graphene bilayer at zero bias voltage, as shown in Figure 3a. Clearly, the spontaneously transferred electrons in the GNF with BN−graphene substrate are obviously less pronounced than that with the graphene substrate (Figure 1a), which indicates that the interlayer interaction is markedly attenuated. To be more substantiated, we also plot the spin-resolved local density of states (LDOS) of the GNF with BN−graphene substrate under different bias voltages in parts a−c of Figure 4. As shown in Figure 4b for the system with zero voltage, the highest-occupied molecular orbital (HOMO) and the lowest-unoccupied molecular orbital (LUMO) are contributed by spin-down and spin-up states of the GNF, respectively. Notably, there is no small DOS peak around the Fermi level, in contrast to the corresponding LDOS in the case of GNF with only graphene substrate as shown in Figure 4d, where both the spin-up and spin-down states have small DOS peaks in the vicinity of the Fermi level.

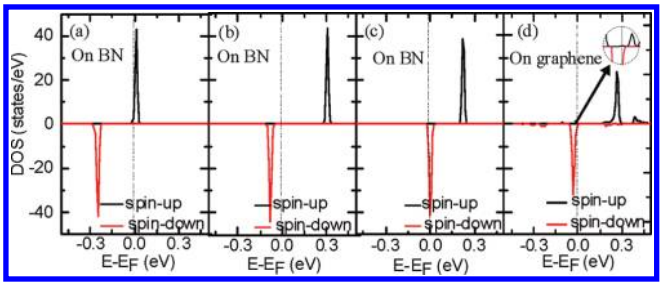

Figure 4. Spin-resolved LDOS of the GNF ($C_{13}H_9$) on BN−graphene substrate under bias voltages (a) 0.60 V/Å, (b) 0 V/Å, and (c) −0.60 V/Å. (d) Spin-resolved LDOS of the GNF on graphene substrate under zero bias voltage.

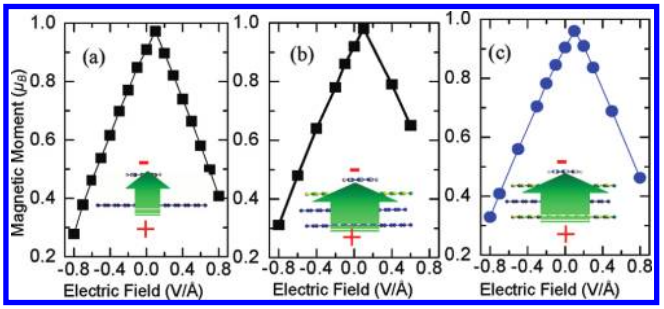

Figure 5. (a) Net magnetic moment of GNF ($C_{13}H_9$) as a function of electric field strength (with a separation of 0.6 nm between the GNF and graphene substrate). (b) Net magnetic moment of GNF on BN−bilayer graphene substrate as a function of electric field strength. (c) Net magnetic moment of GNF on BN−graphene−BN substrate as a function of electric field strength. The graphene is placed on the BN sheet substrate. Inserts are the atomic structure of the corresponding systems with bias electric field. Blue, green, yellow, and gray balls represent carbon, nitride, boron, and hydrogen atoms, respectively.

This underscores the role of interlayer interaction in determining the distribution of electronic states around the Fermi level. As a result, the electrons only fill the HOMO of spin-up states in the *p*-doped region while only depleted from the LUMO of spin-down channel in the *n*-doped region (parts a and b of Figure 4), thus always opening only one spin-polarized channel for the filling of the field driven doping carrier while leaving the carrier occupation of the opposite spin orientation nearly unchanged. This produces a linear ME effect within the calculated range of bias voltages in the system including an intermediate BN layer.

Further calculations show that the ME coefficient increases with increasing the layer number of graphene in the BN-contained system. As shown in Figure 5a, we perform the same ME calculations for the GNF placed on the BN sheet with underlying bilayer graphene substrate. With the bias voltage changing from 0.1 to −0.8 V/Å, the ME coefficient is 3.79×10^{-12} G cm^2/V (see Figure 5b) and larger than 3.67×10^{-12} G cm^2/V of the GNF with single graphene sheet substrate (Figure 3b). This is easy to understand as the increased distance between the flake and the bottom graphene layer would enhance the electric field screening to increase the charge transfer between the graphene and GNF. What's more, we find that the ME effect remains essentially unchanged when the BN-contained system is overall placed on an *h*-BN substrate, as shown in Figure 5c. This suggests that the *h*-BN sheet provide an excellent platform to realize the linear ME effect in the magnetic GNFs. The BN/graphene

dx.doi.org/10.1021/jp205841z |*J. Phys. Chem. C* 2012, 116, 626–631

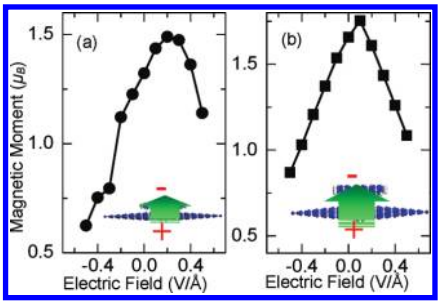

Figure 6. (a) Net magnetic moment of GNF ($C_{54}H_{20}$) on graphene substrate as a function of electric field strength. (b) Net magnetic moment of GNF on graphene substrate as a function of electric field strength (with a separation of 0.60 nm between the GNF and graphene substrate).

sandwiched system is quite realistic in the laboratory by using the related transfer technique, as has been well developed in recent experiments.[41] Therefore, the demonstrated ME systems are completely feasible in experiment and hence should find important realistic applications in future spintronics.

The above results have established that the $C_{13}H_9$ graphene flake can show a nonlinear−linear transition of the ME effect by adjusting the felt interaction of the flake from the substrate. We now prove that this result is not limited to such a piece of a graphene quantum dot and can be extended into other graphene magnets, regardless of its morphology. To illustrate this point, we place a larger GNF ($C_{54}H_{20}$) on the graphene substrate and perform the same ME calculations as above. It is found that the ME effect in $C_{54}H_{20}$ is nonlinear as shown in Figure 6a. Also, this nonlinear ME coupling can be switched to be linear when increasing the distance between the $C_{54}H_{20}$ and graphene substrate (see Figure 6b). In addition, we have also put the magnetic graphene with point defect in plane on graphene substrate, and a near-linear ME effect still appears in such a defect-driven graphene magnets. Overall, our detailed examination on the charge transfer show that the graphene layers in all above systems mainly behave as a source of electrons to facilitate the bias-driven doping in the supported GNFs. In this regard, the graphene should be replaceable by other functional materials, such as SiC, BC_2N sheets, or silicon substrates.

We finally return to the system studied in ref 9, wherein a bilayered graphene nanoribbons adsorbed on silicon substrate is used as the model system. Here, the function of the bottom layer is akin to the BN layer in Figure 3 since this ribbon layer is highly inert due to the interface bonding with the substrate at the ribbon edge. So the top layer suffers a weak interlayer interaction with the bottom ribbon layer, thereby gives a linear ME effect. In contrast, when the bottom layer is replaced by a monolayer graphene, the ME effect becomes nonlinear in the second ribbon layer although the graphene layer also bonds with the substrate. This is because the bonding between the substrate and graphene is highly weakened and hence the graphene electronic states still substantially mix with states in the top ribbon layer.

To this end, one may be curious as to whether the fields used in this study are practically and experimentally useful. It is exciting that the bias voltages of the same order in magnitude as we studied have been experimentally achievable [up to 3 V/nm, see ref 42] and have been used to tune the properties of bilayer graphene. Since the systems in our manuscript are similar to a bilayer graphene, our findings are therefore probably attainable in experiment. Even so, putting the ME effect into device application does not need to switch the magnetism. In many cases, a small quantitative modulation of the system moment is sufficient. Our results show that even a *low* field of 1 V/nm could significantly change the magnetic moment by up to 0.08 μ_B, which meets the requirement of many related devices.

4. SUMMARY AND CONCLUSION

We have explored the bias-induced ME effect in magnetic GNFs placed on lamellar substrates using first-principles calculations. We show that the ME behavior strongly depends on the chemical activity of the substrate on which the magnetic GNF are supported, because the interlayer interaction felt by the GNF can affect the distribution of electronic states around the Fermi level. On the basis of this principle, we realize a nonlinear−linear transition in ME effect through changing the substrate. Notably, we demonstrate that graphene substrate gives a nonlinear ME effect in magnetic GNFs while inserting an intermediate *h*-BN sheet between them can regulate the ME effect to be linear and meanwhile enhance the ME coefficients. Our results offer important insight in guiding experimenters to get linear ME effect and also shed light on applications in advanced ME devices based on sp-element magnetic materials.

AUTHOR INFORMATION

Corresponding Author

*E-mail: wlguo@nuaa.edu.cn (W.G.); chuwazhang@nuaa.edu.cn (Z.Z.).

ACKNOWLEDGMENT

This work is supported by the 973 Program (2007CB936204, 2012CB933403), National NSF (11172124, 10732040, 91023026), and Jiangsu Province NSF (BK2008042, BK2011722) of China and the NUAA Research Fund (4015-YAH10043), National and Jiangsu Postdoctoral Research Foundation (20110490132, 1002015B).

REFERENCES

(1) Rondinelli, J.; Stengel, M.; Spaldin, N. *Nat. Nanotechnol.* **2008**, *3*, 46.
(2) Eerenstein, W.; Mathur, N. D.; Scott, J. F. *Nature* **2006**, *442*, 759.
(3) Fiebig, M. *J. Phys. D: Appl Phys* **2005**, *38*, R123.
(4) Kimura, T.; Goto, T.; Shintani, H.; Ishizaka, K.; Arima, T.; Tokura, Y. *Nature* **2003**, *426*, 55.
(5) Lottermoser, T.; Lonkai, T.; Amann, U.; Hohlwein, D.; Ihringer, J.; Fiebig, M. *Nature* **2004**, *430*, 541.
(6) Duan, C.-G.; Velev, J.; Sabirianov, R. F.; Zhu, Z.; Chu, J; Jaswal, S. S.; Tsymbal, E. Y. *Phys. Rev. Lett.* **2008**, *101*, 137201.
(7) Kamala Bharathi, K.; Markandeyulu, G.; Ramana, C. V. *J. Phys. Chem. C* **2011**, *115*, 554.
(8) Jaiswal, A.; Das, R.; Maity, T.; Vivekanand, K.; Adyanthaya, S.; Poddar, P. *J. Phys. Chem. C* **2010**, *114*, 12432.
(9) Zhang, Z.; Chen, C.; Guo, W. *Phys. Rev. Lett.* **2009**, *103*, 187204.
(10) Zhang, Z.; Chen, C.; Zeng, X. C.; Guo, W. *Phys. Rev. B* **2010**, *81*, 155428.
(11) Güttinger, J.; Frey, T.; Stampfer, C.; Ihn, T.; Ensslin, K. *Phys. Rev. Lett.* **2010**, *105*, 116801.
(12) Saha, S.; Baskey, M.; Majumdar, D. *Adv. Mater.* **2008**, *22*, 5531.
(13) Gao, X.; Wang, L.; Ohtsuka, Y.; Jiang, D.; Zhao, Y.; Nagase, S.; Chen, Z. *J. Am. Chem. Soc.* **2009**, *131*, 9663.
(14) Shemella, P.; Zhang, Y.; Mailman, M. *Appl. Phys. Lett.* **2007**, *91*, 042101.
(15) Jiang, D.; Sumpter, B.; Dai, S. *J. Chem. Phys.* **2007**, *127*, 124703.

(16) Wang, W.; Meng, S.; Kaxiras, E. *Nano Lett.* **2008**, *8*, 241.
(17) Umadevi, D.; Narahari Sastry, G. *J. Phys. Chem. C* **2011**, *115*, 9656.
(18) Soin, N.; Roy, S. S.; Roy, S.; Hazra, K. S.; Misra, D.; Lim, T.; Hetherington, C.; McLaughlin, J. *J. Phys. Chem. C* **2011**, *115*, 5366.
(19) Güçlü, A. D.; Potasz, P.; Voznyy, O.; Korkusinski, M.; Hawrylak, P. *Phys. Rev. Lett.* **2009**, *103*, 246805.
(20) Sheng, W.; Ning, Z. Y.; Yang, Z. Q.; Guo, H. *Nanotechnology* **2010**, *21*, 385201.
(21) Yazyev, O.; Wang, W.; Meng, S.; Kaxiras, E. *Nano Lett.* **2008**, *8*, 766.
(22) Silva, A. M.; Pires, M. S.; Freire, V. N.; Albuquerque, E. L.; Azevedo, D. L.; Caetano, E. W. S. *J. Phys. Chem. C* **2010**, *114*, 17472.
(23) Kresse, G.; Hafner, J. *Phys. Rev. B* **1993**, *47*, 558–561.
(24) Kresse, G.; Hafner, J. *Phys. Rev. B* **1994**, *49*, 14251–14269.
(25) Kresse, G.; Furthmuller, J. *Phys. Rev. B* **1996**, *54*, 11169–11186.
(26) B3LYP functional:(a) Becke, A. D. *J. Chem. Phys.* **1993**, *98*, 5648. (b) Lee, C.; Yang, W.; Parr, R. G. *Phys. Rev. B* **1988**, *37*, 785.
(27) Frisch, M. J.; Trucks, G. W.; Schlegel, H. B.; Scuseria, G. E.; Robb, M. A.; Cheeseman, J. R.; Montgomery, J. A., Jr.; Vreven, T.; Kudin, K. N.; Burant, J. C.; Millam, J. M.; Iyengar, S. S.; Tomasi, J.; Barone, V.; Mennucci, B.; Cossi, M.; Scalmani, G.; Rega, N.; Petersson, G. A.; Nakatsuji, H.; Hada, M.; Ehara, M.; Toyota, K.; Fukuda, R.; Hasegawa, J.; Ishida, M.; Nakajima, T.; Honda, Y.; Kitao, O.; Nakai, H.; Klene, M.; Li, X.; Knox, J. E.; Hratchian, H. P.; Cross, J. B.; Bakken, V.; Adamo, C.; Jaramillo, J.; Gomperts, R.; Stratmann, R. E.; Yazyev, O.; Austin, A. J.; Cammi, R.; Pomelli, C.; Ochterski, J. W.; Ayala, P. Y.; Morokuma, K.; Voth, G. A.; Salvador, P.; Dannenberg, J. J.; Zakrzewski, V. G.; Dapprich, S.; Daniels, A. D.; Strain, M. C.; Farkas, O.; Malick, D. K.; Rabuck, A. D.; Raghavachari, K.; Foresman, J. B.; Ortiz, J. V.; Cui, Q.; Baboul, A. G.; Clifford, S.; Cioslowski, J.; Stefanov, B. B.; Liu, G.; Liashenko, A.; Piskorz, P.; Komaromi, I.; Martin, R. L.; Fox, D. J.; Keith, T.; Al-Laham, M. A.; Peng, C. Y.; Nanayakkara, A.; Challacombe, M.; Gill, P. M. W.; Johnson, B.; Chen, W.; Wong, M. W.; Gonzalez, C.; Pople, J. A. *Gaussian 03*, revision C.02; Gaussian, Inc.: Wallingford, CT, 2004.
(28) Lieb, E. *Phys. Rev. Lett.* **1989**, *62*, 1201.
(29) Yazyev, O V. *Rep. Prog. Phys.* **2010**, *73*, 056501.
(30) Novoselov, K. S.; Jiang, D.; Schedin, F.; Booth, T. J.; Khotkevich, V. V.; Morozov, S. V.; Geim, A. K. *Proc. Natl. Acad. Sci. U.S.A.* **2005**, *120*, 10451.
(31) Guo, Y.; Guo, W.; Chen, C. *Appl. Phys. Lett.* **2008**, *92*, 243101.
(32) With the bias voltage changing from −0.2 to 0.7 V/Å, the Dirac point can deviate from the Fermi level in the spin-unresolved band structure induced by the charge transfer from the graphene. However, along with the spin polarization of nanoflake, the Fermi level of the system can be raised (lowered) when the nanoflake is *n*-type (*p*-type) doped. Therefore, the Dirac point still meets the Fermi level in a spin-resolved band structure.
(33) Jin, C.; Lin, F.; Suenaga, K.; Iijima, S. *Phys. Rev. Lett.* **2008**, *102*, 195505.
(34) Dean, C. R.; Young, A. F.; Meric, I.; Lee, C.; Wang, L.; Sorgenfreil, S.; Watanabe, K.; Taniguchi, T.; Kim, P.; Shepard, K. L.; Hone, J. *Nat. Nanotechnol.* **2010**, *5*, 722.
(35) Duan, C.-G.; Jaswal, S. S.; Tsymbal, E. Y. *Phys. Rev. Lett.* **2006**, *97*, 047201.
(36) Laukhin, V.; Skumryev, V.; Marti, X.; Hrabovsky, D.; Sanchez, F.; Garcia-Cuenca, M. V.; Ferrater, C.; Varela, M.; Luders, U.; Bobo, J . F.; Fontcuberta, J. *Phys. Rev. Lett.* **2006**, *97*, 227201.
(37) Weisheit, M.; Fähler, S.; Marty, A.; Souche, Y.; Poinsignon, C.; Givord, D. *Science* **2007**, *315*, 349.
(38) Eerenstein, W.; Wiora, M.; Prieto, J. L.; Scott, J. F.; Mathur, N. D. *Nat. Mater.* **2007**, *6*, 348.
(39) Tsymbal, E. Y.; Hermann, K. *Science* **2007**, *313*, 181.
(40) Gajek, M.; Bibes, M.; Fusil, S.; Bouzehouane, K.; Fontcuberta, J.; Barthelemy, A.; Fert, A. *Nat. Mater.* **2007**, *6*, 296.
(41) Xue, J.; Sanchez-Yamagishi, J.; Bulmash, D.; Jacquod, P.; Deshpande, A.; Watanabe, K.; Taniguchi, T.; Jarillo-Herrero, P.; LeRoy, B. J. *Nat. Mater.* **2011**, *10*, 282.
(42) Zhang, Y.; Tang, T.-T.; Girit1, C.; Hao, Z.; Martin, M. C.; Zettl, A.; Crommie, M. F.; Ron Shen, Y.; Wang, F. *Nature* **2009**, *459*, 820.